

High spatial resolution spectroscopy of Tycho's SNR with *Chandra*

Yun-Dong Guo and Xue-Juan Yang

School of Physics and Optoelectronics, Xiangtan University, Xiangtan 411105, China; xjyang@xtu.edu.cn

Received 2016 March 21; accepted 2016 October 21

Abstract We present high spatial resolution X-ray spectroscopy of Tycho's supernova remnant (SNR) using observational data from *Chandra*. The whole remnant was divided into 26×27 regions, with each of them covering $20'' \times 20''$. We selected 536 pixels with enough events to generate spectra and fit them with an absorbed two component non-equilibrium ionization model. We obtained maps of absorbing column density, weight-averaged temperature, ionization age and abundances for O, Ne, Mg, Si, S and Fe, with emission used to determine the weight. The abundance maps and the finding that Fe abundance is not correlated with any other element suggest that Fe is located at a smaller radius than other elements, supporting the onion shell model with emission from more massive elements peaking more toward the center. A tight correlation between Si and S abundances support both Si and S coming from explosive O-burning and/or incomplete Si-burning. O and Ne abundances show no correlation with any other element. Considering that O, Ne and Mg are all synthesized in the same process (C/Ne-burning), we suggest that O/Ne/Mg might mix well with other elements during the explosion of the supernova and the expansion of the SNR.

Key words: ISM: supernova remnants — ISM: individual (Tycho)

1 INTRODUCTION

The remnant of supernova 1572 (SN 1572) recorded by Tycho Brahe, also known as Tycho's supernova remnant (SNR), is a standard Type Ia remnant. Recent studies suggest its distance to be 2.5 – 3 kpc (Tian & Leahy 2011). It has been extensively observed at all wavelengths (Kirshner et al. 1987; Teske 1990, Smith et al. 1991 in optical; Dickel et al. 1991, Wood et al. 1992 in radio; Acciari et al. 2011 in gamma ray). There is a general agreement that Type Ia supernovae (SNe) originate from the thermonuclear explosion of a white dwarf that accretes material from its close companion star to the Chandrasekhar mass limit. This single-degenerate scenario is supported by the discovery of a possible surviving companion (Ruiz-Lapuente et al. 2004) and the observation of a unique X-ray arc/shadow originating from the impact of the SN ejecta and the stripped envelope of the companion star (Lu et al. 2011). However, the details of the explosion are still under debate.

As a young SNR, its X-ray emission is relatively bright and mostly dominated by the shocked ejecta. Therefore, abundant emission lines have been detected in

the soft X-ray band, including O, Ne, Mg, Si, S, Ar, Ca, Cr, Mn, Fe, etc (Tsunemi et al. 1986; Smith et al. 1988; Hwang & Gotthelf 1997; Decourchelle et al. 2001; Yang et al. 2009; Tamagawa et al. 2009). By taking images from emission energy ranges associated with different elements, it has also been suggested that the elements are stratified in Tycho's SNR, with lighter elements located at larger radii and Fe in the innermost region (Hwang & Gotthelf 1997; Aschenbach 2002). This represents strong evidence supporting the onion shell model with the dominant elements ordered in shells according to their atomic number (Stadlbauer & Aschenbach 2001). Thanks to the high spatial resolution and long working-life of *Chandra* and *XMM-Newton*, the expansion and dynamics of this SNR can be studied with observational data (Hughes 2000; Hayato et al. 2010; Katsuda et al. 2010). Moreover, high spatial resolution spectroscopy is also possible (Willingale et al. 2002; Yang et al. 2008, 2014). Recently, Li et al. (2015) and Luna et al. (2016) developed a self-adaptive method to perform spatially resolved spectroscopy on SN 1006 and Puppis A. In this paper, we present systematic spectroscopy of Tycho's SNR region by region.

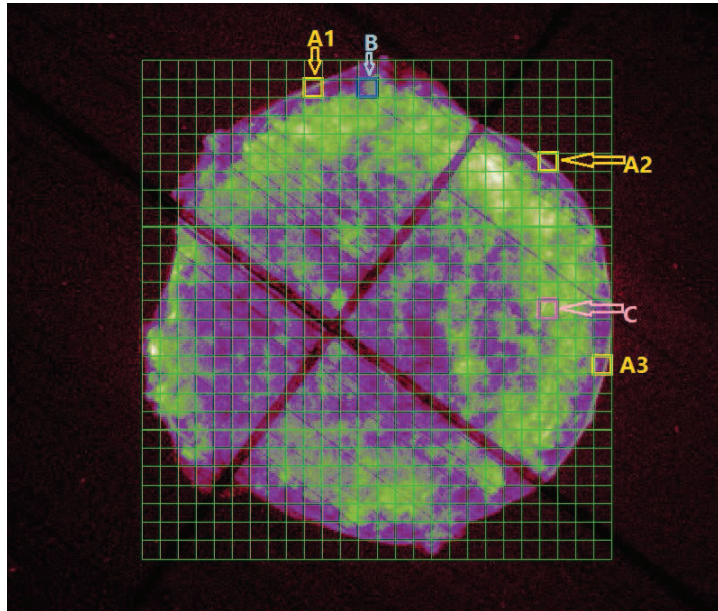


Fig. 1 The pixel grid used in our analyses superimposed on the *Chandra* image of Tycho’s SNR. Several typical regions are marked: three *yellow boxes* (A1, A2 and A3) represent the forward shocked rim, while *blue* and *magenta boxes* (B and C respectively) correspond to reverse shocked ejecta.

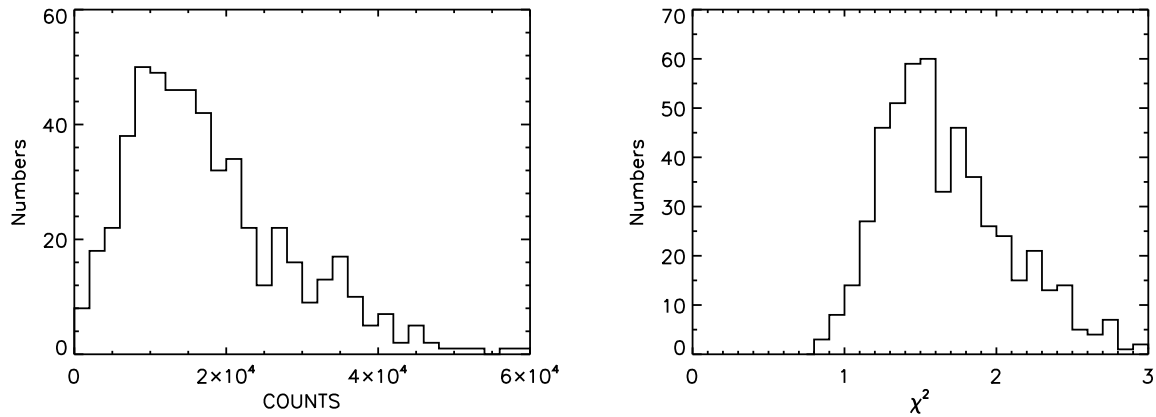


Fig. 2 Frequency distribution of the total counts from the 536 pixels (*left panel*) and χ^2 values (*right panel*) obtained in the spectral fitting.

2 OBSERVATION AND DATA REDUCTION

In this work, we analyze *Chandra* observation with ID 3837. This observation was acquired on 2003-04-29 from 02:00:50 to 19:25:41 UTC. The Advanced CCD Imaging Spectrometer (ACIS)-I was used to record this observation. We applied the standard data reduction for the level-1 event data with CALDB version 3.4.0. The net exposure time was about 145 ks after standard screening.

The X-ray data were analyzed using the software package CIAO (version 4.3). In the present work, we divided the X-ray emission region into 26×27 grids with

“pixel” size $20'' \times 20''$. 536 pixels out of all the 702 grids with enough events were selected to produce spectra within the energy range 0.5–10 keV.

Figure 1 shows the image of this observation with the grid overlaid. The background spectrum was created from the off-source region. The average count for all the 536 regions was ~ 18000 , and 450 of them contained more than 8000 counts. Figure 2 (*left panel*) shows the distribution of the total counts for each region.

The spectra were fitted with the XSPEC software package (version 12.5.0, Arnaud 1996), using two non-equilibrium ionization components (VNEI version 1.1,

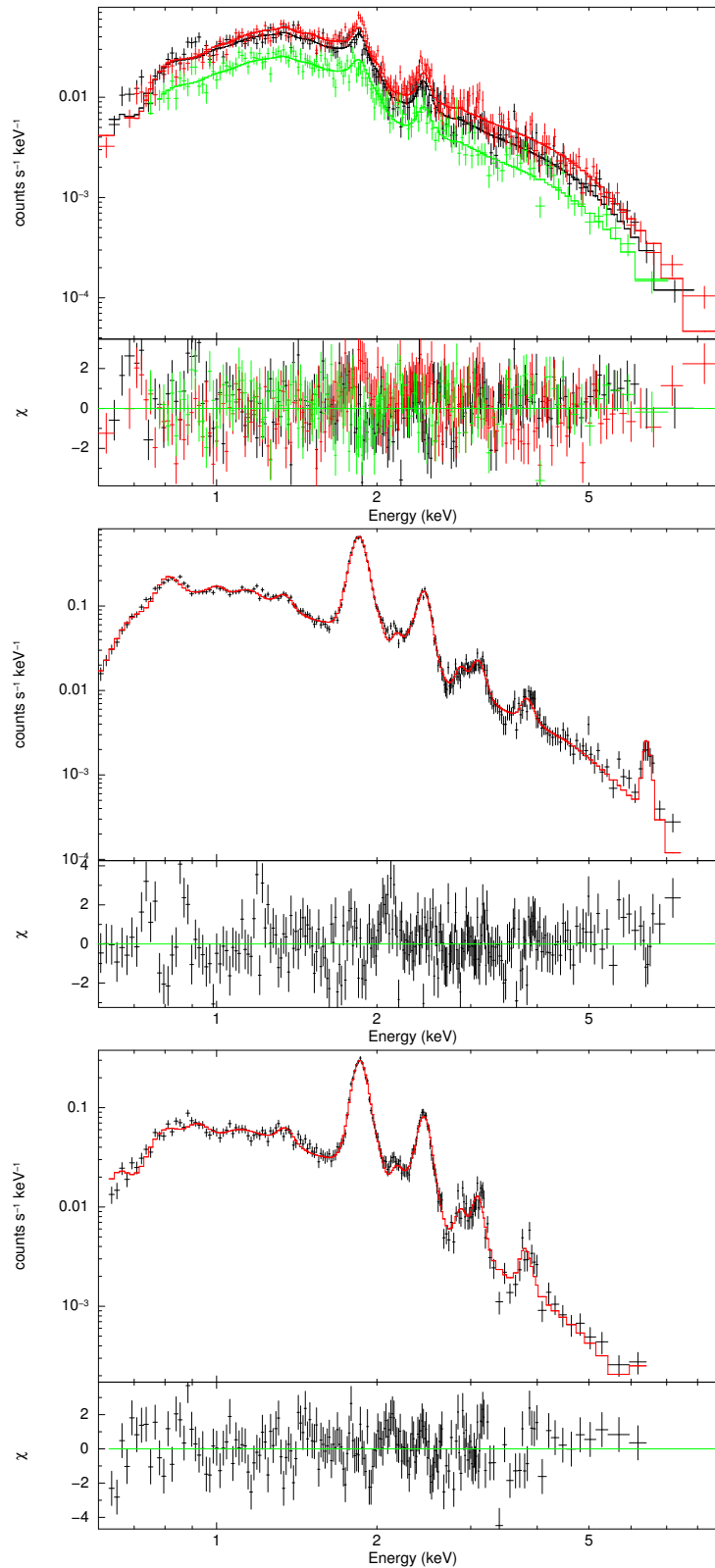


Fig. 3 Spectra along with fitting results for typical regions: *top panel*: spectra of regions A1 (*black*), A2 (*red*) and A3 (*green*); *middle panel*: spectrum of region B; *bottom panel*: spectrum of region C. In the middle and bottom panel, black represents the observation data points and red the fitting model.

Borkowski et al. 2001). Interstellar photoelectric absorption was taken into account with the WABS model (Morrison & McCammon 1983). The free parameters are the absorption column density, temperatures, emission measures, ionization ages ($\tau = n_e t$) and abundances of O, Ne, Mg, Si, S, Ca and Fe (in units of solar abundances given by Anders & Grevesse (1989) for each VNEI component. The reason these elements’ abundances are free is that they show prominent emission lines in the spectra (cf. Fig. 3). A Gaussian component was added with the line center energy of about 3.1 keV to take care of the Ar emission line. We note here that we have also tried other models such as an absorbed one VNEI component and VNEI plus powerlaw model. It turns out that the two-temperature VNEI model can best describe spectra statistically and physically. The typical errors for Si, S and Fe abundances are about 10%–20%, and 40%–50% for O, Ne, Mg and Ca abundances. In the following discussion, all the fitted parameters except the absorption column density are the weighted averages of the two components with emission used to determine the weight.

A histogram of the 536 reduced χ^2 values of the spectral fits is shown in Figure 2 (right panel). It has a peak around 1.45, suggesting the fitting results to be statistically acceptable.

3 SPECTRA OF DIFFERENT REGIONS

Figure 3 shows the spectra and fitting residuals of three kinds of typical regions as marked in Figure 1.

Regions A1, 2 and 3 cover the forward shocked interstellar medium (ISM) filaments in three different directions, i.e. northwest (NW), northeast (NE) and southwest (SW) respectively. Such kinds of filaments are not prominent in the southern part of the SNR in the current observation. The spectra of the three regions are very similar to each other. They are all dominated by the continuum, and only weak Si and S lines can be observed (cf. Fig. 3, bottom panel), just as expected as their origin is shocked ISM. Such kinds of filaments are very typical in young SNRs. Along with the SN explosion, the forward shock is formed and will expand in interstellar space. It will interact with the ISM and form such kinds of filaments at the outer edge of an SNR (Cassam-Chenaï et al. 2007).

Regions B and C are both located in the bright shell inside the ISM filaments. Their spectra show properties that are typical of shocked ejecta, with strong emission lines of metal elements, such as Ne, Mg, Si, S, Ar, Ca and Fe. The abundances for these elements are basically several times the solar value. The clearest difference between the two spectra is that Region B shows strong emission from Fe K lines but Region C does not show

them. Moreover, the Fe L line in Region B is also much stronger than that in Region C. Such Fe-rich ejecta is common in young SNRs, especially in Type Ia cases, because in a Type Ia SN the whole progenitor is destroyed to form the SNR, including the Fe nuclei.

4 SPATIAL DISTRIBUTION OF THE FITTED PARAMETERS

Figure 4 presents the spatial distribution of the absorbing column density, temperature and ionization ages. The absorbing column density to Tycho’s SNR basically lies in the range of $0.6 - 1.2 \times 10^{22} \text{ cm}^{-2}$, with an average value around $0.8 \times 10^{22} \text{ cm}^{-2}$. This is generally consistent with previous results within the confidence range (Warren et al. 2005).

The temperatures are typically 0.7 – 1.5 keV. It is clearly shown that at the outer rim the plasma is relatively hot. Also, the observation used to generate the ionization time scale ($\log_{10} n_e t$) map leads to the conclusion that the outer rim has a much higher ionization time scale than the inner regions.

Here we caution the reader that these outer rims are dominated by synchrotron filaments and the continuum is strongly contaminated by synchrotron emission (Cassam-Chenaï et al. 2007). Therefore, the best-fit temperatures and ionization time scales are strongly affected by the presence of the nonthermal continuum and might not be reliable.

It has been suggested in several papers that Fe ejecta lies at a smaller radius than the other elements. Based on spectroscopy targeting Tycho’s SNR, Hwang et al. (1998) found that Fe K ejecta has a temperature at least two times higher and an ionization age 100 times lower than that of Si/S, suggesting that Fe ejecta was shocked more recently. From the X-ray images of Mg, Si, S and Fe, Aschenbach (2002) showed that Fe ejecta lies at a smaller radius than the other elements. Badenes et al. (2006) also suggest that Fe peak elements lie interior to intermediate-mass elements, based on a comparison between spatially integrated X-ray spectra and SN Ia explosion models. Miceli et al. (2015) found indications for a stratification of the abundances of Ca and Fe K from the equivalent width (EW) maps.

These results are basically taken from images of associated elements, spatially integrated spectra, or the EW map. Here we show in the abundance map that Fe is located at a smaller radius than other elements in this remnant (cf. Fig. 5). This further supports the onion shell model with emission from more massive elements peaking more toward the center.

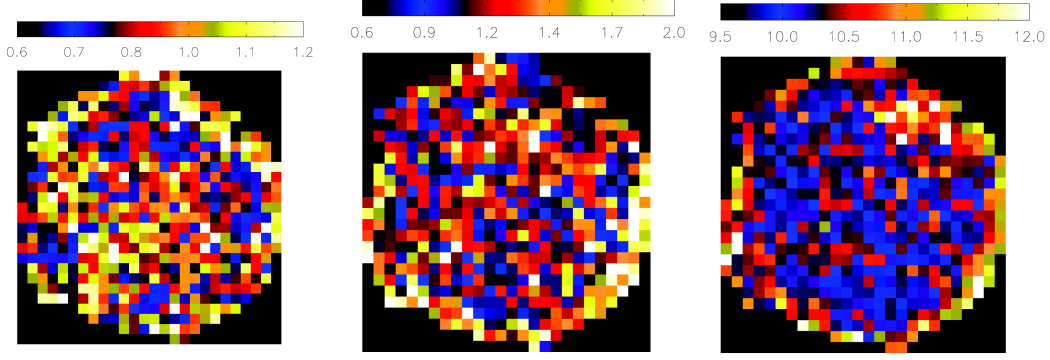


Fig. 4 The absorbing column density (N_{H} , 10^{22} cm^{-2} , *left panel*), temperature (kT , keV, *middle panel*) and ionization age ($\log_{10} n_e t \text{ cm}^{-3} \text{ s}$, *right panel*) maps of Tycho's SNR. The coding used is shown on the top of each panel.

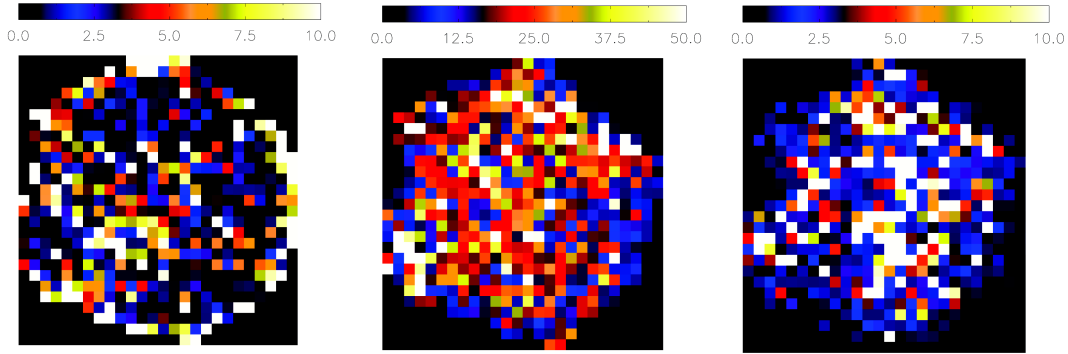


Fig. 5 O (*left*), Si (*middle*), and Fe (*right*) abundance (in units of solar abundance) maps of Tycho's SNR. The typical error for O abundance is 40% – 50%, and 10% – 20% for Si and Fe abundances.

Table 1 Coherence coefficient for data points excluding extremum ones. The corresponding values for Cas A (Yang et al. 2008) are given in parentheses.

Element	O	Ne	Mg	Si	S	Fe
O	–	0.13(0.33)	0.15(0.41)	0.28(0.33)	0.19(0.26)	0.17(0.13)
Ne	0.13(0.33)	–	0.04(0.49)	0.34(0.19)	0.09(0.16)	0.07(0.25)
Mg	0.15(0.41)	0.04(0.49)	–	0.09(0.48)	0.24(0.39)	0.19(0.24)
Si	0.28(0.33)	0.34(0.19)	0.09(0.48)	–	0.49(0.86)	0.06(0.23)
S	0.19(0.26)	0.09(0.16)	0.24(0.39)	0.49(0.86)	–	0.09(0.11)
Fe	0.17(0.13)	0.07(0.25)	0.19(0.24)	0.06(0.23)	0.09(0.11)	–

5 CORRELATIONS OF THE ELEMENT ABUNDANCES

Figures 6 and 7 show the correlation plots of the abundances of O and Ne, and Si and Fe with other elements. The minimum points ($\sim 30\%$ of the total data points) are excluded, because they basically represent regions whose spectra are dominated by the continuum. These spectra show relatively weak metal emission lines and thus the abundances are very small. The coherence coefficients

are given in Table 1. We would like to make a comparison with the corresponding values of SNR Cassiopeia A (Cas A), as Tycho's SNR and Cas A represent SNRs from Type Ia and core-collapse SNe respectively.

Based on Figures 6 and 7 and Table 1, we can come to the following conclusions:

- (1) The relatively light elements O and Ne show no correlation with any other element. This is different from Cas A and G292.0+1.8. In Cas A the Ne and

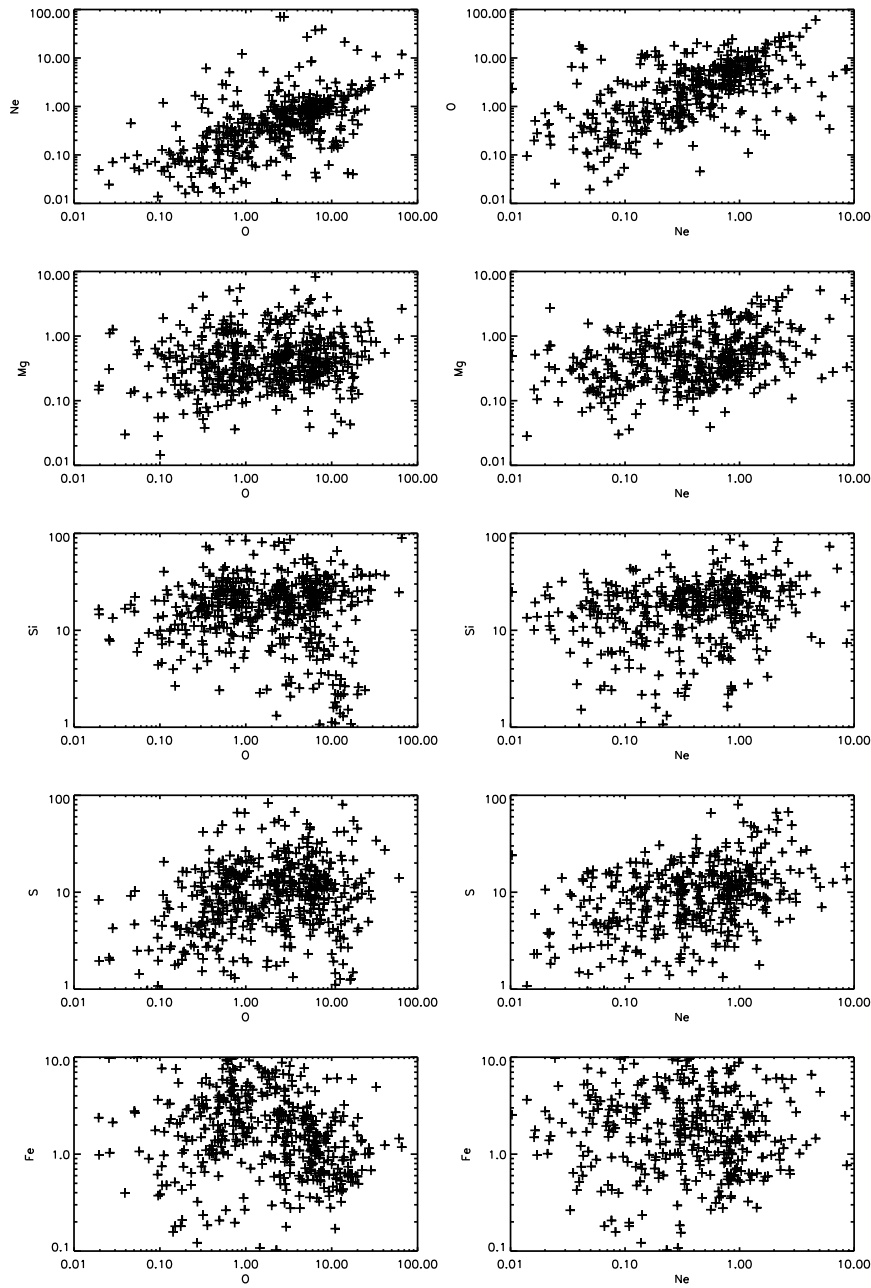


Fig. 6 Abundance correlation between O/Ne and other elements.

Mg abundances are positively correlated to a certain degree (Yang et al. 2008), while in the O-rich SNR G292.0+1.8, the abundances of O, Ne and Mg are correlated tightly with each other (Yang et al. 2014). The correlation pattern can easily be understood, since these elements are abundant in this SNR and they all come from the same nucleosynthesis process. In Tycho’s SNR, no such correlation is observed, probably for two reasons: one is that these elements are well mixed, and the other is that the

emission lines of these elements in Tycho’s SNR are relatively weak, making the abundance not well constrained from the spectral fitting, thus increasing the scatter in the correlation.

- (2) The abundances of medium-mass elements Si and S are well correlated with each other, just as in Cas A and G292.0+1.8 (Yang et al. 2008, 2014). Such a correlation indicates that they both come from explosive O-burning and/or incomplete Si-burning. In addition, Si and S have been suggested to be spatially

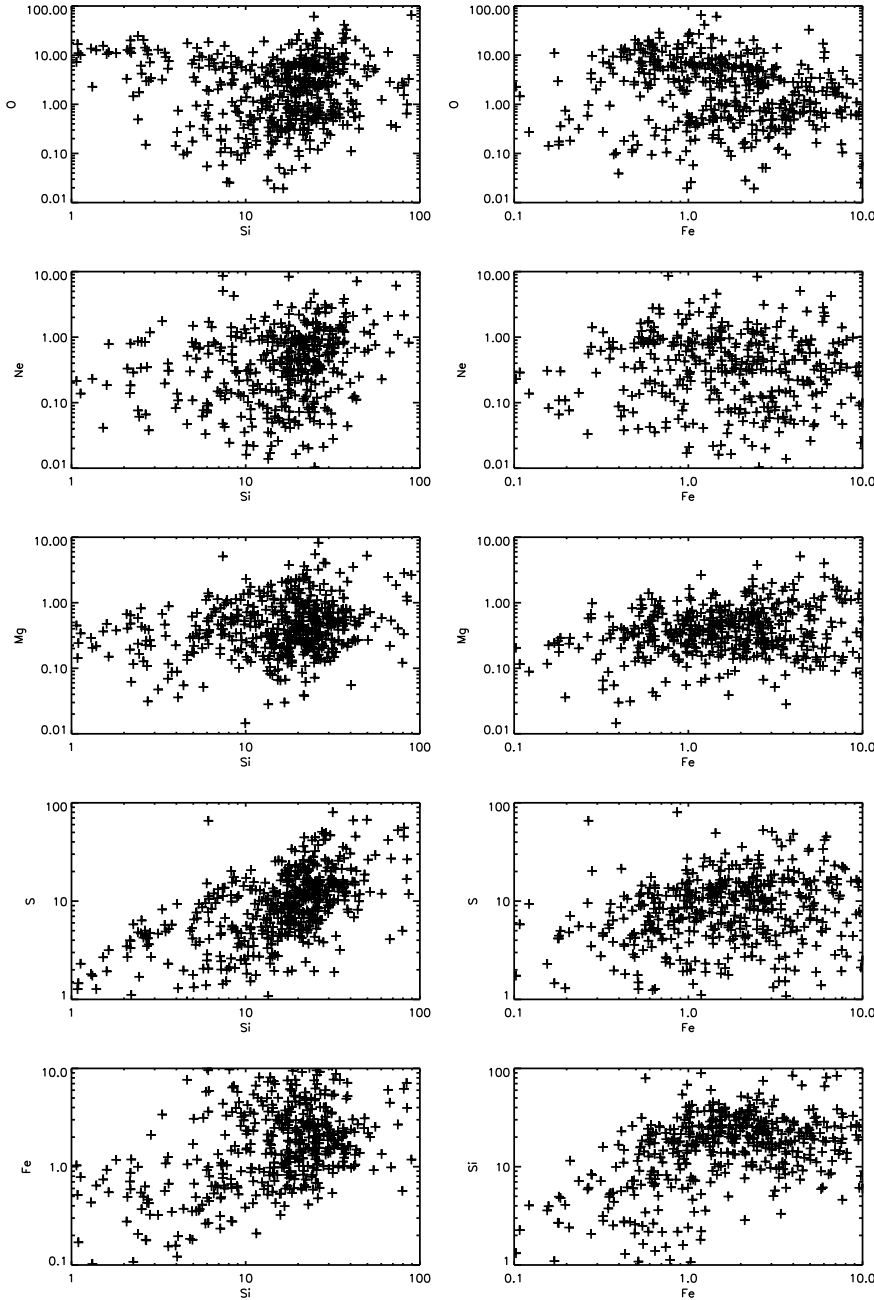


Fig. 7 Abundance correlation between Si/Fe and the other elements.

co-located in Tycho's SNR (Aschenbach 2002). For the above two reasons, it is natural that their abundances are positively correlated.

- (3) The Fe abundance shows no correlation with any other elements. The reason might be that Fe is located in the innermost region in Tycho's SNR (Aschenbach 2002) and it is not spatially correlated with any other element.

6 SUMMARY

We present high spatial resolution X-ray spectroscopy of Tycho's SNR using *Chandra* observation data. With the spectral analysis results we obtained maps of absorbing column density, weight-averaged temperature, ionization age and abundances for O, Ne, Mg, Si, S and Fe, with emission used to measure the weight. The abundance maps suggest that Fe is located at a smaller radius than

other elements, supporting the onion shell model with the emission from more massive elements peaking more toward the center. In addition, Fe abundance is not correlated with any other element, suggesting that Fe is not co-located with other element. We find a tight correlation between Si and S abundances, just as seen in SNRs Cas A and G292.0+1.8. This result supports both Si and S coming from explosive O-burning and/or incomplete Si-burning. O and Ne abundances show no correlation with any other element. Considering that O, Ne and Mg are all synthesized in the same process (C/Ne-burning), we suggest that O/Ne/Mg might mix well with other elements during the explosion of the SN and the expansion of the SNR.

Acknowledgements We acknowledge the use of data obtained by *Chandra*. The Chandra Observatory Center is operated by the Smithsonian Astrophysical Observatory for and on the behalf of NASA. This project is supported by the National Natural Science Foundation of China (NSFC, Grant No. 11473023) and Hunan Provincial Natural Science Foundation (2015JJ3124).

References

- Acciari, V. A., Aliu, E., Arlen, T., et al. 2011, *ApJ*, 730, L20
- Anders, E., & Grevesse, N. 1989, *Geochim. Cosmochim. Acta*, 53, 197
- Arnaud, K. A. 1996, in *Astronomical Society of the Pacific Conference Series*, 101, *Astronomical Data Analysis Software and Systems V*, eds. G. H. Jacoby, & J. Barnes, 17
- Aschenbach, B. 2002, in *Neutron Stars, Pulsars, and Supernova Remnants*, ed. W. Becker, H. Lesch, & J. Trümper, 13
- Badenes, C., Borkowski, K. J., Hughes, J. P., Hwang, U., & Bravo, E. 2006, *ApJ*, 645, 1373
- Borkowski, K. J., Lyerly, W. J., & Reynolds, S. P. 2001, *ApJ*, 548, 820
- Cassam-Chenaï, G., Hughes, J. P., Ballet, J., & Decourchelle, A. 2007, *ApJ*, 665, 315
- Decourchelle, A., Sauvageot, J. L., Audard, M., et al. 2001, *A&A*, 365, L218
- Dickel, J. R., van Breugel, W. J. M., & Strom, R. G. 1991, *AJ*, 101, 2151
- Hayato, A., Yamaguchi, H., Tamagawa, T., et al. 2010, *ApJ*, 725, 894
- Hughes, J. P. 2000, *ApJ*, 545, L53
- Hwang, U., & Gotthelf, E. V. 1997, *ApJ*, 475, 665
- Hwang, U., Hughes, J. P., & Petre, R. 1998, *ApJ*, 497, 833
- Katsuda, S., Petre, R., Hughes, J. P., et al. 2010, *ApJ*, 709, 1387
- Kirshner, R., Winkler, P. F., & Chevalier, R. A. 1987, *ApJ*, 315, L135
- Li, J.-T., Decourchelle, A., Miceli, M., Vink, J., & Bocchino, F. 2015, *MNRAS*, 453, 3953
- Lu, F. J., Wang, Q. D., Ge, M. Y., et al. 2011, *ApJ*, 732, 11
- Luna, G. J. M., Smith, M. J. S., Dubner, G., Giacani, E., & Castelletti, G. 2016, *A&A*, 590, A70
- Miceli, M., Sciortino, S., Troja, E., & Orlando, S. 2015, *ApJ*, 805, 120
- Morrison, R., & McCammon, D. 1983, *ApJ*, 270, 119
- Ruiz-Lapuente, P., Comeron, F., Méndez, J., et al. 2004, *Nature*, 431, 1069
- Smith, A., Davelaar, J., Peacock, A., et al. 1988, *ApJ*, 325, 288
- Smith, R. C., Kirshner, R. P., Blair, W. P., & Winkler, P. F. 1991, *ApJ*, 375, 652
- Stadlbauer, T. F. X., & Aschenbach, B. 2001, in *Astronomical Society of the Pacific Conference Series*, 251, *New Century of X-ray Astronomy*, eds. H. Inoue, & H. Kunieda, 276
- Tamagawa, T., Hayato, A., Nakamura, S., et al. 2009, *PASJ*, 61, 167
- Teske, R. G. 1990, *ApJ*, 362, 563
- Tian, W. W., & Leahy, D. A. 2011, *ApJ*, 729, L15
- Tsunemi, H., Yamashita, K., Masai, K., Hayakawa, S., & Koyama, K. 1986, *ApJ*, 306, 248
- Warren, J. S., Hughes, J. P., Badenes, C., et al. 2005, *ApJ*, 634, 376
- Willingale, R., Bleeker, J. A. M., van der Heyden, K. J., Kaastra, J. S., & Vink, J. 2002, *A&A*, 381, 1039
- Wood, C. A., Mufson, S. L., & Dickel, J. R. 1992, *AJ*, 103, 1338
- Yang, X.-J., Lu, F.-J., & Chen, L. 2008, *ChJAA* (Chin. J. Astron. Astrophys.), 8, 439
- Yang, X.-J., Liu, X.-Q., Li, S.-Y., & Lu, F.-J. 2014, *RAA* (Research in Astronomy and Astrophysics), 14, 1279
- Yang, X. J., Tsunemi, H., Lu, F. J., et al. 2009, *ApJ*, 692, 894